Scientia Iranica B (2023) 30(3), 1008–1026

SCIENTIA IRANICA

Sharif University of Technology
**Scientia Iranica**
*Transactions B: Mechanical Engineering*
http://scientiairanica.sharif.edu

*Research Note*

# Effect of turbulent and laminar flow mechanisms on airflow patterns and $CO_2$ distribution in an operating room: A numerical analysis abbreviated title: Airflow pattern in an operating room

**V. Gholami Motlagh[a,*], M. Ahmadzadehtalatapeh[a], and O. Mohammadi[b,c]**

a. *Department of Mechanical Engineering, Chabahar Maritime University, Chabahar, Iran.*
b. *Department of Mechanical Engineering, Sharif University of Technology, Tehran, Iran.*
c. *Department of Mechanical Engineering, University of British Columbia, 6250 Applied Science Ln, Vancouver, BC, Canada.*

Received 8 November 2021; received in revised form 20 April 2022; accepted 5 December 2022

**KEYWORDS**
Air distribution;
Computational Fluid Dynamic (CFD);
$CO_2$ concentration;
HVAC system;
Operating room.

**Abstract.** Considering the risk of infection in surgeries, maintaining an acceptable indoor air quality in Operating Rooms (ORs) to ensure the health and safety of patients and surgical team is very essential. Since airflow is one of the primary mechanisms for transmitting infections and pollution, it is crucial to examine the air distribution systems in the ORs. In the present study, the effect of Turbulent and Laminar Airflow (TAF/ LAF) systems on the air and $CO_2$ distribution in an OR was examined. The effects of inlet and outlet configurations were evaluated for seven different models. The results indicate that the LAF systems are superior to TAF systems. Based on the findings, the LAF with the air curtain configuration brings about the minimum $CO_2$ concentration level in the OR. The results showed that LAF with the air curtain model could reduce the $CO_2$ concentration by about 64.66% and 88.96% on the central plane, which passes along the body patient on 1.14 m and 1.7 m above the floor, respectively, compared to the existing model.



## 1. Introduction

Surgical Site Infections (SSIs) of an incision, organ, or space normally occur after a surgery [1]. SSIs are among the most challenging post-operative healthcare complications that significantly contribute to increased mortality, prolonged hospitalization, and surgery repeat [2,3]. SSIs increase healthcare costs [4–6]. SSIs are the most common hospital infections among the surgical patients and account for 38% of the infections. In addition, 77% of surgical patients who died from hospital infections were SSI-related cases [7]. Literature indicates that the main source of Bacteria-Carrying Particles (BCPs) in Operating Rooms (ORs) was the surgical team. It was also confirmed that airborne BCPs were dependent on the number of people in the OR, and the dispersal of skin bacteria varied from person to person [8–11]. Patient and surgical staff respiration emissions are one of the factors that causes OR pollution. $CO_2$ is produced in the OR by the exhalation of patient and surgical staff. It is

*. *Corresponding author.*
*E-mail addresses: v_gholami@yahoo.com (V. Gholami Motlagh); m_ahmadzadeh56@yahoo.com (M. Ahmadzadehtalatapeh); omidmohmm@gmail.com (O. Mohammadi)*

doi: 10.24200/sci.2022.59351.6192

recommended that $CO_2$ concentration should be below 1500 ppm (< 1500 ppm) [12].

The proper design of OR ventilation for the patient and surgical team is essential. Heating, Ventilation, and Air Conditioning (HVAC) systems play a vital role in providing optimal conditions and minimizing air pollution risk in ORs. In addition to ventilation systems, other measures such as disinfection of the surgical wound, regular cleaning of the OR, disinfection of hands, and the use of medical gloves are effective in reducing SSIs [13].

The purpose of the air distribution study in the OR is to protect the patient and surgical team against infection and establish comfort [13]. Primary surgeries are usually performed in hospital wards; however, this pattern changed dramatically in the 18th century by employing the operating theaters to improve the surgery educations [14,15]. In 1946, one of the first studies on wound infection and airborne bacteria was published [14,15]. In the 1980s, the focus of OR design shifted to Ultra Clean Ventilation (UCV) systems. This concept originated from the electronic and aerospace industries, which require particle-free environments [7]. Major studies showed that these systems could significantly reduce the number of bacteria in the OR and risk of deep sepsis compared to conventional air conditioners [14,16,17]. However, recent studies have shown that the basis for this focus is not very accurate. In 2017, Bischoff et al. [18] concluded that UCV had no advantage over the conventional ventilation systems in terms of SSIs control.

Andersson et al. [19] described the importance of Laminar Airflow (LAF) in the OR as a protection against SSIs. It was shown that the LAF pattern provided acceptable air quality during the operation with a very low level of Colony-Forming Units (CFUs) near the surgical bed. The differences in air contamination quality in the LAF and displacement flow patterns were also examined. The effects of the number of people in the OR and air movement were also investigated. Wang et al. [20] numerically examined the temperature-controlled airflow against the turbulent mixing and LAF for OR ventilation systems. In this study, the effect of a ventilation scheme was explored to reduce the distribution of BCPs and deposition in the OR. The results showed that temperature-controlled airflow represented a safe and suitable ventilation. In comparison to LAF systems, this system can provide an energy-efficient solution. In addition, increasing the ventilation rate alone does not necessarily improve the distribution of BCPs. Furthermore, it was proved that airflow patterns contributed to the removal and dilution of airborne BCPs. The effect of door opening and closing on the airflow of the OR was investigated by Alonso et al. [21]. The aim of this study was to quantify the air flow that entered the OR during the door opening and closing. In this study, two ORs, one with a Turbulent Airflow (TAF) system and the other with a LAF system, were investigated. Also, the effect of two types of doors, namely hinged and sliding, on the air quality of the OR was investigated. The results of this study illustrated that the process of the door opening and closing led to the entry of air from surrounding areas into the OR in all of the studied cases regardless of the type of ventilation system used. All test cases showed that sliding doors reduced incoming air from surrounding areas. Therefore, sliding doors are considered as the preferred options in ORs in order to reduce the entry of outside air into the OR.

Gholami Motlagh and Ahmadzadehtalatapeh [22] examined the air distribution patterns in an OR in Iran. In this research, the distribution of temperature, humidity, velocity, and respiratory flow patterns of the patient and the surgical team were explored. The results showed that LAF systems were highly capable of controlling the comfort parameters, compared to TAF systems. It was also shown that LAF systems were more effective in controlling and guiding the respiratory flow of patients and the surgical team outside the Surgical Zone (SZ) than the TAF systems. Liu et al. [23] investigated the diffusion of BCPs in the OR owing to the interaction between the human thermal column and ventilation systems. Different ventilation systems including vertical LAF ventilation, horizontal LAF ventilation, and temperature-controlled airflow ventilation were employed to compare and evaluate the diffusion of human thermal plume and BCPs. The results showed that both the vertical LAF and temperature-controlled airflow systems had the capability to interact effectively with the human thermal plume and the temperature-controlled airflow system was superior to other systems in reducing the level of BCPs in the OR air. It was also demonstrated that the temperature-controlled airflow system reduced the concentration of BCPs in the SZ up to 20 $CFU/m^3$.

Literature survey indicates that mixing ventilation and LAF systems are the most widely used ventilation systems in ORs. Generally, it is believed that the LAF system removes bacteria more effectively [24]. Despite extensive valuable research on the subject, there are still many shortcomings to recommend a complete ventilation system for the ORs. Therefore, comparative research studies still required to determine a fully efficient ventilation system for ORs. To this end, the present study comparatively examines three ventilation systems including LAF, TAF, and LAF with air curtain systems. In the present research, three ventilation systems with different inlet and outlet configurations are evaluated to propose the most suitable design to create comfortable air conditions for the patient and staff.

## 2. Research methodology

### 2.1. Model geometry

The present study investigates the air distribution in the OR of Iranian Surgery Clinic, Chabahar, Iran. The considered OR is used for general surgery and it is located between adjacent rooms. The OR overview, dimensions, and the validation locations, i.e., A, B, C, and D, are given in Figure 1 [22].

Figure 2 shows the existing OR model (model 1). TAF ventilation system is used in the OR. Two wardrobes for medical equipment and medicines are shown with two gray blocks that are located beside the eastern wall. The OR has four circular inlets on the soffit and eight rectangular outlets at the chamfered corners. The dimensions of the inlets and outlets and OR equipment such as ceiling lights, surgical bed, and surgical lights are given in Table 1.

In order to improve the OR's internal atmosphere, several designs and different patterns, namely models 1 to 7, were studied. Models 2 to 4 are related to TAF systems; models 5 and 6 related to LAF systems, and model 7 related to LAF with the air curtain system. The dimensions, number of inlet diffusers and outlet vents, and ACH values for the models are given in Table 2.

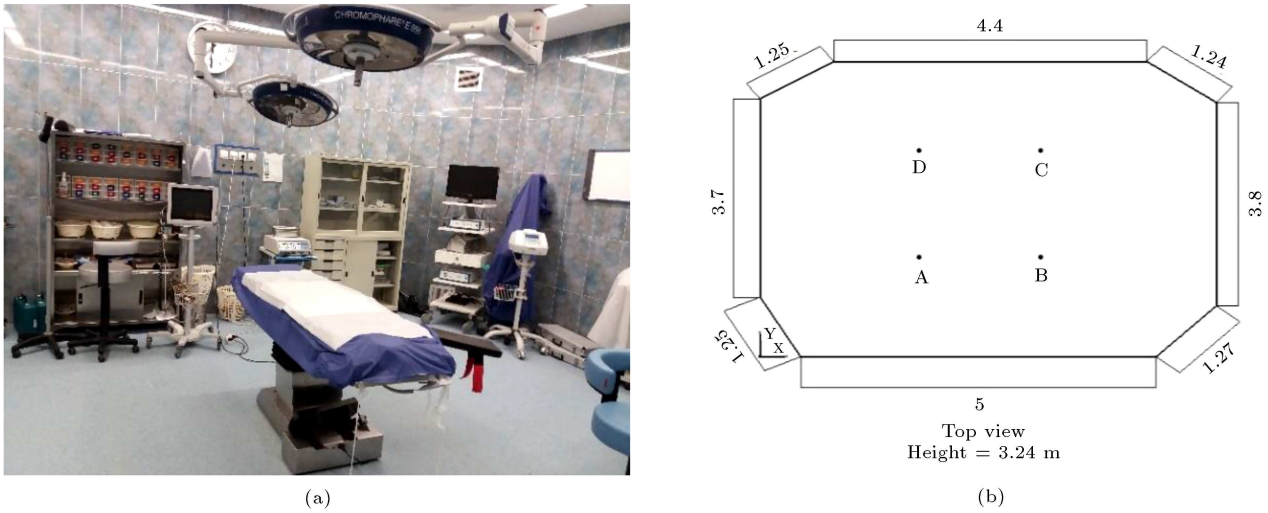


(a) (b)

**Figure 1.** The OR overview: (a) Interior view and (b) The dimensions of the OR (in meter) and location of the validation axes.

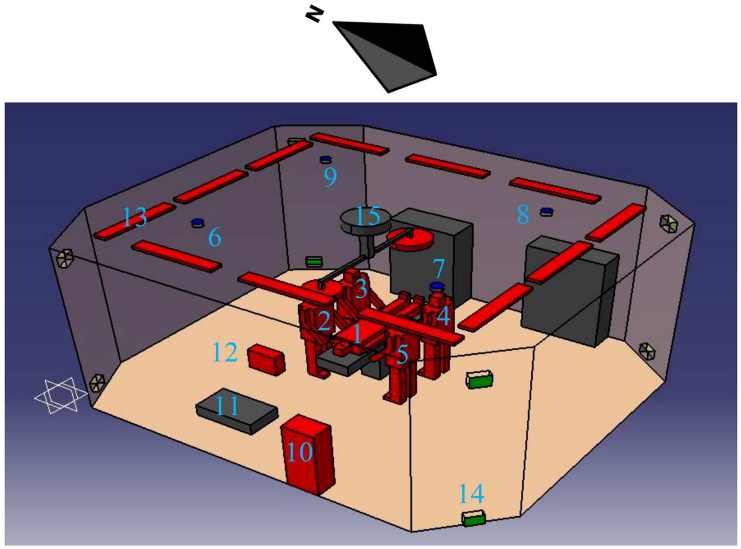


1: Patient
2: Anesthetist
3: Nurse 2
4: Nurse 1
5: Surgeon
6: Inlet 1
7: Inlet 2
8: Inlet 3
9: Inlet 4
10: Anesthesia machine
11: Medical equipment table
12: Patient care monitor
13: Fluorescent
14: Exhaust
15: Light surgery

**Figure 2.** Isometric view of the OR.

**Table 1.** The dimensions of the equipment, mannequins, and inlet and outlet of the OR (Figure 2).

| Item | Quantity | Dimension (m) |
|---|---|---|
| Surgical bed | 1 | 0.5 × 1.98 × 0.2 |
| The basis of the surgical bed | 1 | 0.305 × 0.35 × 0.68 |
| Anesthesia machine | 1 | 0.46 × 0.315 × 1.22 |
| Surgical light 1 | 1 | 0.6 diameter ×0.1 |
| Surgical light 2 | 1 | 0.51 diameter ×0.1 |
| Human model | 5 | 1.7 height |
| Mouth | 5 | 0.04 × 0.02 |
| Patient care monitor | 1 | 0.42 × 0.17 × 0.36 |
| Medical equipment table | 1 | 0.83 × 0.49 × 0.2 |
| Each pair of lamps | 12 | 1.2 × 0.19 × 0.05 |
| Medical equipment wardrobe | 1 | 1.18 × 0.4 × 1.81 |
| Medicine wardrobe | 1 | 1.1 × 0.5 × 1.7 |
| Inlet diffuser | 4 | 0.146 diameter |
| Outlet vent | 8 | 0.235 × 0.185 |
| OR (all the models) | 7 | Figure 1(b) |

**Table 2.** Dimensions and number of inlets and outlets and ACH for design models.

| Model number | | | Quantity | Dimension (m) | ACH |
|---|---|---|---|---|---|
| Model 1 | | Inlet | 4 | 0.146 diameter | 5.87 |
| | | Outlet | 8 | 0.235 × 0.185 | |
| Model 2 | | Inlet | 4 | 0.27 diameter | 20 |
| | | Outlet | 4 | 0.235 × 0.185 | |
| Model 3 | | Inlet | 4 | 0.27 diameter | 20 |
| | | Outlet | 4 | 0.235 × 0.185 | |
| Model 4 | | Inlet | 4 | 0.27 diameter | 20 |
| | | Outlet | 4 | 0.235 × 0.185 | |
| Model 5 | | Inlet | 4 | 0.62 × 1.2 | 20 |
| | | Outlet | 8 | 0.235 × 0.185 | |
| Model 6 | | Inlet | 4 | 1.2 × 0.62 | 20 |
| | | Outlet | 8 | 0.235 × 0.185 | |
| Model 7 | Inlet | Main diffuser | 1 | 1.11 × 2.59 | 31.6 |
| | | Air curtain | 1 | 0.502 $m^2$ | |
| | | Outlet | 8 | 0.235 × 0.185 | |

In the considered models, dimensions, geometry, and locations for placing the equipment and thermal manikins are constant. In models 2 to 4, the area of inlet diffusers and outlet vents is fixed and only the outlet vents have different layouts. For the three mentioned models, four outlet vents are utilized for the OR. In model 2, the outlet vents are installed near the floor. In model 3, the outlet vents are installed so that two of them are near the floor and the two others are near the ceiling. In model 4, the outlet vents are installed near the ceiling. In models 5 to 7, the effect of diffuser layout on airflow distribution has been evaluated in the study. Models 5 and 6 are related to the layouts of $2 \times 2$ and $1 \times 4$ arrays for inlet diffusers, respectively. Model 7 shows the LAF with the air curtain layout for the OR. In this model, a large area of diffuser supplies the OR's main airflow, and a narrow plane around the main diffuser is modeled to create an air curtain. In this model (model 7), the air curtain forms a barrier around the SZ, preventing contaminants from entering. In this system (model 7), 60 to 75% of the overall air inlet must be supplied through the air curtain and the remainder through the main inlet. In this model, the main inlet must be at least 1 foot away from the air curtain to avoid major flow penetration into the air curtain and turbulence flow formation [25]. On the other hand, the ASHRAE standard [26] defines the main diffuser area on the ceiling directly above the surgical bed with a one-foot distance from the sides. The dimensions and location of the equipment and inlet diffusers are illustrated in Figure 3.

### 2.2. Theoretical formulation

The continuity, momentum, energy equations, standard $k$-$\varepsilon$ model, and equation for species transport [27–29] are the essential equations needed to be considered for airflow distribution studies in the OR.

The continuity equation is defined as follows:

$$\nabla \cdot \rho \vec{v} = -\frac{\partial \rho}{\partial t}. \tag{1}$$

The equation for momentum is:

$$\frac{\partial}{\partial t}(\rho \vec{v}) + \nabla \cdot (\rho \vec{v} \vec{v}) = -\nabla P + \nabla \cdot (\overline{\overline{\tau}}) + \rho \vec{g}. \tag{2}$$

In addition, the equation for energy is:

$$\frac{\partial}{\partial t}(\rho E) + \nabla \cdot (\vec{v}(\rho E + P)) = \nabla \cdot (\rho K_{eff} \nabla T - h + (\overline{\overline{\tau}}_{eff} \cdot \vec{v})). \tag{3}$$

$E$ is defined as Eq. (4):

$$E = h - \frac{p}{\rho} + \frac{V^2}{2}. \tag{4}$$

The Boussinesq approximation is defined as follows:

**Table 3.** Coefficients the standard $k - \varepsilon$ model.

| Coefficient | $C_\mu$ | $C_{1\varepsilon}$ | $C_{2\varepsilon}$ | $\sigma_k$ | $\sigma_\varepsilon$ |
|---|---|---|---|---|---|
| Value | 0.09 | 1.44 | 1.92 | 1 | 1.3 |

$$\rho_\beta = \rho_o(1 - \beta \cdot \Delta T). \tag{5}$$

Eq. (5) defines the Boussinesq approximation and also, the thermal expansion coefficient ($\beta$) is defined by Eq. (6) as follows:

$$\beta = -\frac{1}{\rho}\frac{\partial \rho}{\partial T} = \frac{1}{T}. \tag{6}$$

The equations for turbulent kinetic energy and dissipation rate are presented as follows:

$$\frac{\partial}{\partial x_i}(\rho k u_i) = \frac{\partial}{\partial x_i}\left[\left(\mu + \frac{\mu_t}{\sigma_k}\right)\frac{\partial k}{\partial x_i}\right] + G_k + G_b - \rho\varepsilon - Y_M + S_k, \tag{7}$$

$$\frac{\partial}{\partial x_i}(\rho \varepsilon u_i) = \frac{\partial}{\partial x_i}\left[\left(\mu + \frac{\mu_t}{\sigma_\varepsilon}\right)\frac{\partial \varepsilon}{\partial x_i}\right] + C_{1\varepsilon}\frac{\varepsilon}{k}(G_k + C_{3\varepsilon}G_b) - \rho C_{2\varepsilon}\frac{\varepsilon^2}{k} + S_\varepsilon. \tag{8}$$

Table 3 [30] presents the standard $k - \varepsilon$ model coefficients.

The equation for species transport is:

$$\frac{\partial(\rho \overline{Y_i u_j})}{\partial x_j} = \frac{\partial}{\partial x_j}\left((D + D_t)\frac{\partial \overline{Y_i}}{\partial x_j}\right) + S_i. \tag{9}$$

### 2.3. Numerical method

To solve the momentum, energy, turbulent kinetic energy, pressure velocity coupling, and dissipation rate equations, the commercial software ANSYS Fluent 19 was used. The conservation equations were solved using the finite element method for the steady-state condition, and pressure-based solver was used for the simulations. Moreover, the second-order method was used to discretize the momentum, energy, and turbulence conservation equations [31,32]. The RNG $k - \varepsilon$ model is applicable and recommended for displacement airflow [33], but for an OR, due to the relative low level turbulence, the standard $k - \varepsilon$ model is more applicable for predicting the airflow [33,34]. Therefore, the standard $k - \varepsilon$ model was employed to solve the air distribution. For natural convection, the Boussinesq approximation was used and the SIMPLE algorithm was utilized for pressure and velocity coupling. The convergence criterion for the energy was considered as $1 \times 10^{-6}$ and $1 \times 10^{-3}$ for continuity, velocity, $k$, and $\varepsilon$ [31]. Convergence criterion for other species was set at $1 \times 10^{-3}$.

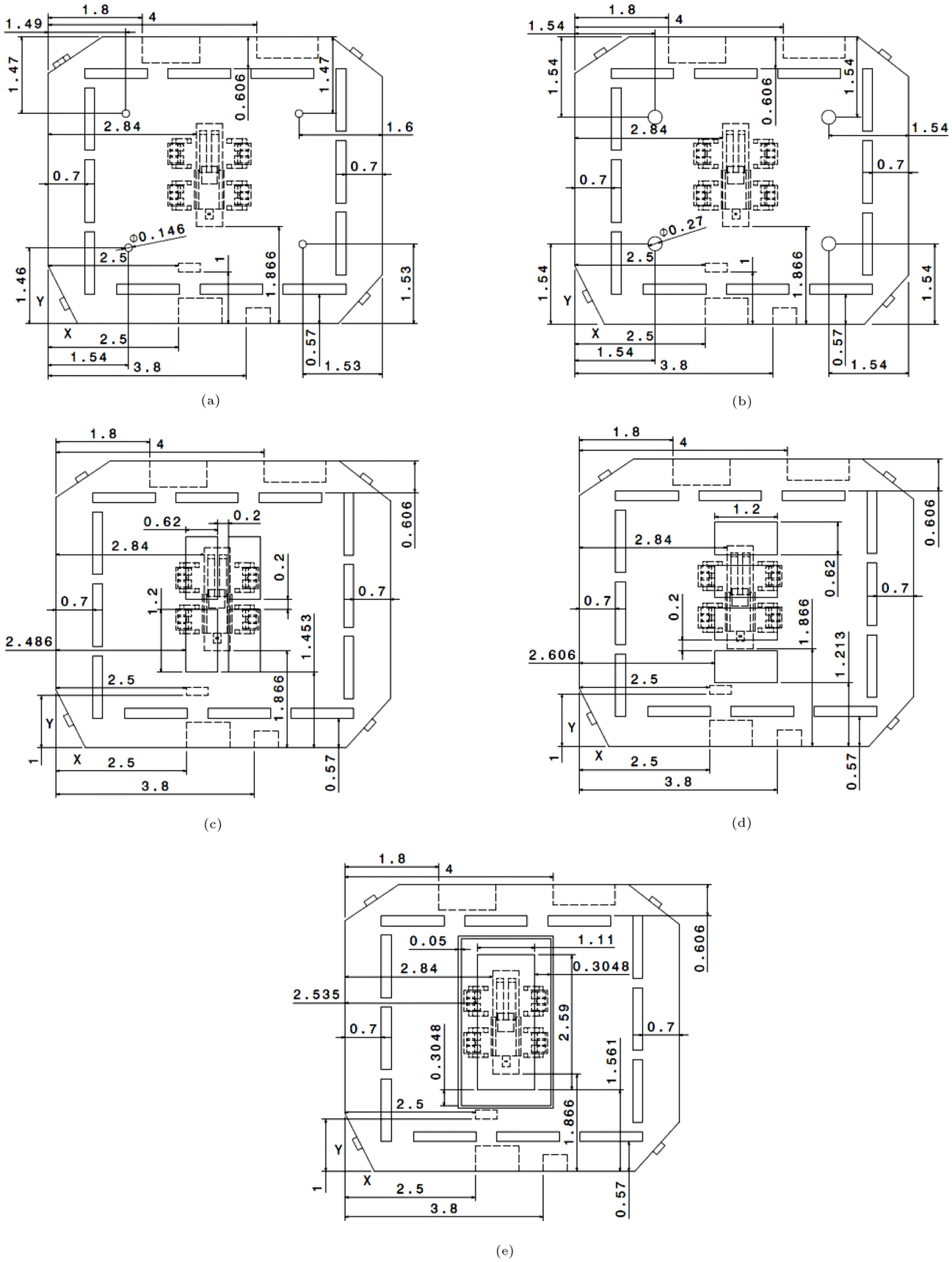


**Figure 3.** The dimensions and location of the equipment and inlet diffusers (in meter): (a) Model 1, (b) model 2, 3 & 4, (c) model 5, (d) model 6, and (e) model 7.

### 2.4. Grid study

Considering a high quality mesh for a simulation is essential and the quality of the computational mesh has a significant effect on Computational Fluid Dynamic (CFD) simulation performance [25]. The OR model with different mesh numbers, namely 695,821; 976,418; 1,520,563; 2,700,374 at two central planes ($X = 3.09$ m and $Y = 2.866$ m) was analyzed. The generated mesh for the room model is shown in Figure 4.

The mean temperature variation at two central planes ($X = 3.09$ m and $Y = 2.866$ m) for different mesh numbers is shown in Figure 5. As shown in Figure 5, the parameter difference for the mesh numbers of 1,520,563 and 2,700,374 cells is negligible. Therefore, the mesh with 1.5 million cells is desired for the OR, and the simulations were performed under this mesh number.

### 2.5. Boundary conditions

Based on the fieldwork measurements, the boundary conditions are defined. The supply air inlet conditions were modeled as a combination of vapor and dry air without chemical reaction [30]. The supply air

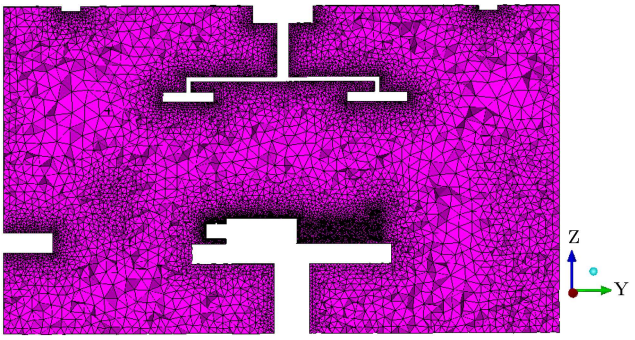


**Figure 4.** Generated mesh for the computational domain: Sectional view of the mesh for computational domain.

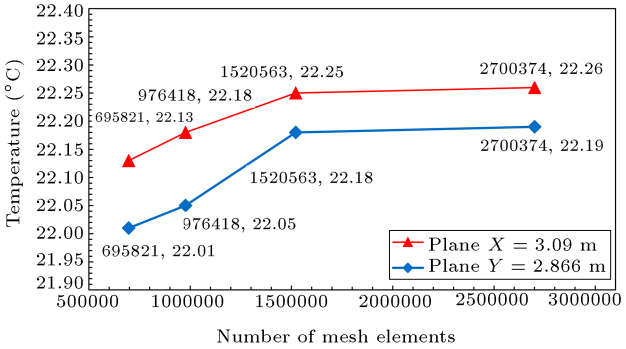


**Figure 5.** Mean air temperature at central planes ($X = 3.09$ m and $Y = 2.866$ m) for different mesh numbers.

enters into the room vertically downwards through the diffusers in the ceiling. $CO_2$ was considered as the only respiratory pollutant by the patient and the staff, and it is released in a mass fraction of $2 \times 10^{-4}$ [30] and flow rate of 8 lit/min [34].

The inlet boundary conditions for the designed models are tabulated in Table 4. The difference in boundary conditions for model 1 is because of the fact that the boundary conditions are determined in this model by the fieldwork measurements. Actually, model 1 is the existing model of the OR, whose boundary conditions are determined by the fieldwork measurements. In order to correctly compare the results of the models, the temperature boundary conditions in models 2 to 7 were considered constant and their values were considered to be adherent to the ASHRAE standards. Since the OR has been located in adjoining rooms and the difference in the temperature between the outside and inside the room is negligible, a constant temperature was assumed for the walls. Table 5 shows the boundary conditions used for the OR walls determined by the fieldwork measurements. Manikin models are heat sources for the room space

**Table 4.** The inlet diffusers' boundary condition.

| Model number | Boundary | Velocity (m/s) | Temperature (°C) |
|---|---|---|---|
| Model 1 | Inlet 1 | 3.4 | 19.9 |
| | Inlet 2 | 2.2 | 21.8 |
| | Inlet 3 | 1.2 | 22.3 |
| | Inlet 4 | 3.6 | 21.1 |
| Model 2, model 3 & model 4 | Inlets | 2.6 | 18.3 |
| Model 5 & model 6 | Inlets | 0.2 | 18.3 |
| Model 7 | Main diffuser | 0.127 | 18.3 |
| | Air curtain | 1.14 | |

**Table 5.** The walls boundary condition.

| Wall | N | S | E | W | C | F | N.E | N.W | S.E | S.W |
|---|---|---|---|---|---|---|---|---|---|---|
| Temperature (°C) | 22.6 | 22.1 | 22.3 | 22.5 | 22.3 | 22.2 | 22.2 | 22.3 | 22.5 | 22.5 |

Note: N. Northern; S. Southern; E. Eastern; W. Western; C. Ceiling; F. Floor; N.E. Northeast; N.W. Northwest; S.E. Southeast; S.W. Southwest.

**Table 6.** Heat sources in the OR space.

| Item | Quantity | Heat source (W) |
|---|---|---|
| Surgical team | 4 | 100 |
| Patient | 1 | 75 |
| Anesthesia machine | 1 | 200 |
| Patient care monitor | 1 | 100 |
| Each pair of lamps | 12 | 16 |
| Surgical lights | 2 | 42 |

and as a consequence, they generate heat energy; therefore, thermal effect must be considered. Other equipment pieces such as patient care monitor, ceiling lamps, surgical lamps, and anesthesia machine are also known as the heat sources. Table 6 shows the values of heat sources in the OR.

### *2.6. Validation*

In order to reliably apply the numerical results, it is necessary to validate the simulation results to confirm their accuracy first. Therefore, to validate and verify the simulation results, the fieldwork measurements were compared to the simulation results. Validation was performed for the existing OR model (model 1). The model was validated based on temperature values on four vertical axes A, B, C, and D (Figure 1). Table 7 shows the coordinates of the validation axes.

Figure 6 illustrates the comparison between simulation and fieldwork measurements values for temperature. Based on Figure 6, the simulation values have acceptable accuracy with a maximum deviation of about 0.8°C. Validation of the velocity values was also ensured to further enhance the credibility of the simulations (Figure 7). An acceptable deviation was observed between the simulation and fieldwork measurements values for the velocity parameter, with the maximum amount of 8.91%.

**Table 7.** Validation axes' coordinates.

| | Coordinate | |
|---|---|---|
| Axis | $x$ | $y$ |
| A | 2.24 | 1.866 |
| B | 3.94 | 1.866 |
| C | 3.94 | 3.846 |
| D | 2.24 | 3.846 |

## 3. Result and discussion

### *3.1. Flow pattern*

Figure 8 shows the airflow pattern for the considered models. In models 1 to 4 (Figure 8), as the TAF models, the air flows into the space through the inlet diffusers vertically and moves to the floor because of its high velocity. A fraction of the inlet flow is discharged through the outlet vents, and another portion moves to the SZ after encountering with the floor. The airflow density decreases due to the heat exchange with the existing heat sources and it moves upward. The airflow of the SZ is pushed up to the inlet diffusers and mixes with the inlet air. This movement increases the contamination and concentration of particles in the area and exposes the patient and the surgical team to the polluted air. Such ventilation systems are not recommended for ORs because of ineffective performance in removing infections and indoor pollution.

Figure 8 also illustrates the path lines of models 5 to 7 as the LAF systems. It was shown that these models would provide a fully controllable flow pattern for the SZ. In these models, the ceiling diffusers are located above the patient's body and the surgical team. The inlet air moves directly to the SZ and provides fresh air for the personnel and patients. In model 7, due to the existence of air curtain, it guides the main diffuser flow uniformly towards the patient and the surgical team. Due to the high velocity of the linear diffusers compared to the main diffuser, they create a curtain of air around the main diffuser and the SZ. The air curtain acts as a physical barrier and prevents the

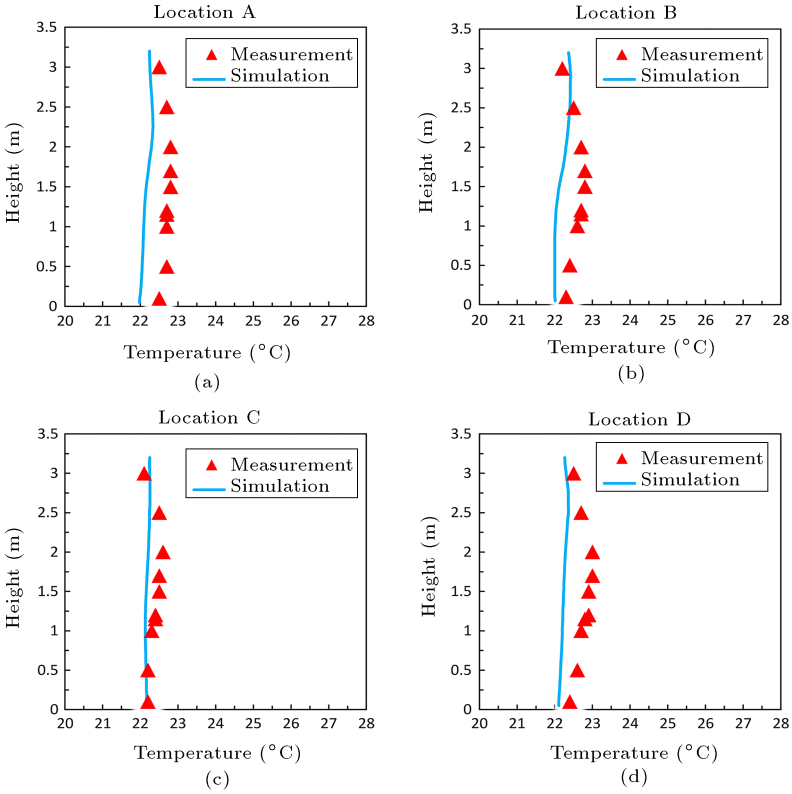


**Figure 6.** The simulation and fieldwork measurements values for temperature: (a) Axis A, (b) axis B, (c) axis C, and (d) axis D.

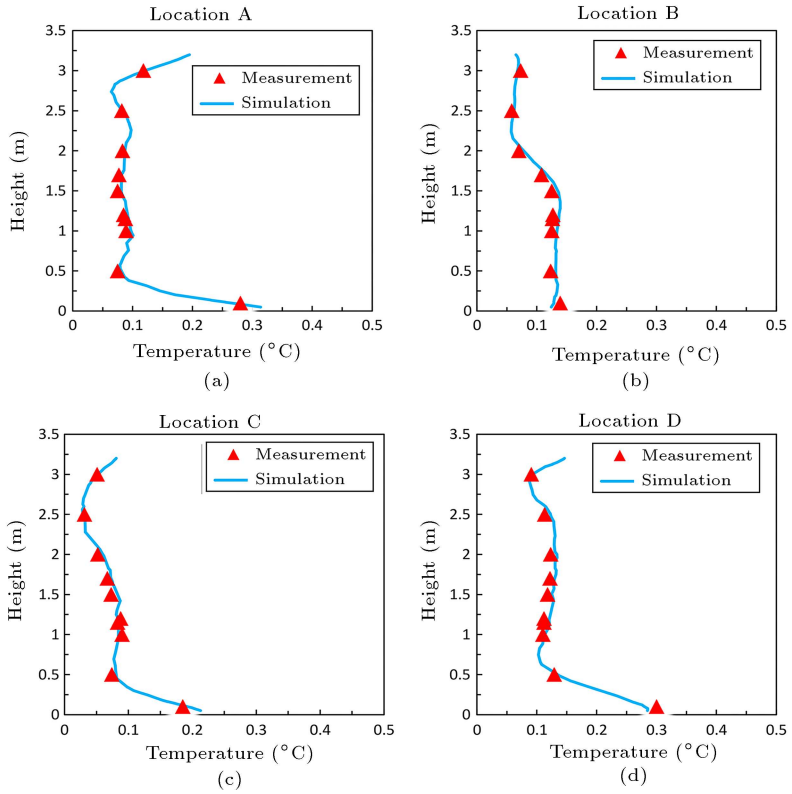


**Figure 7.** The simulation and fieldwork measurements values for velocity: (a) Axis A, (b) axis B, (c) axis C, and (d) axis D.

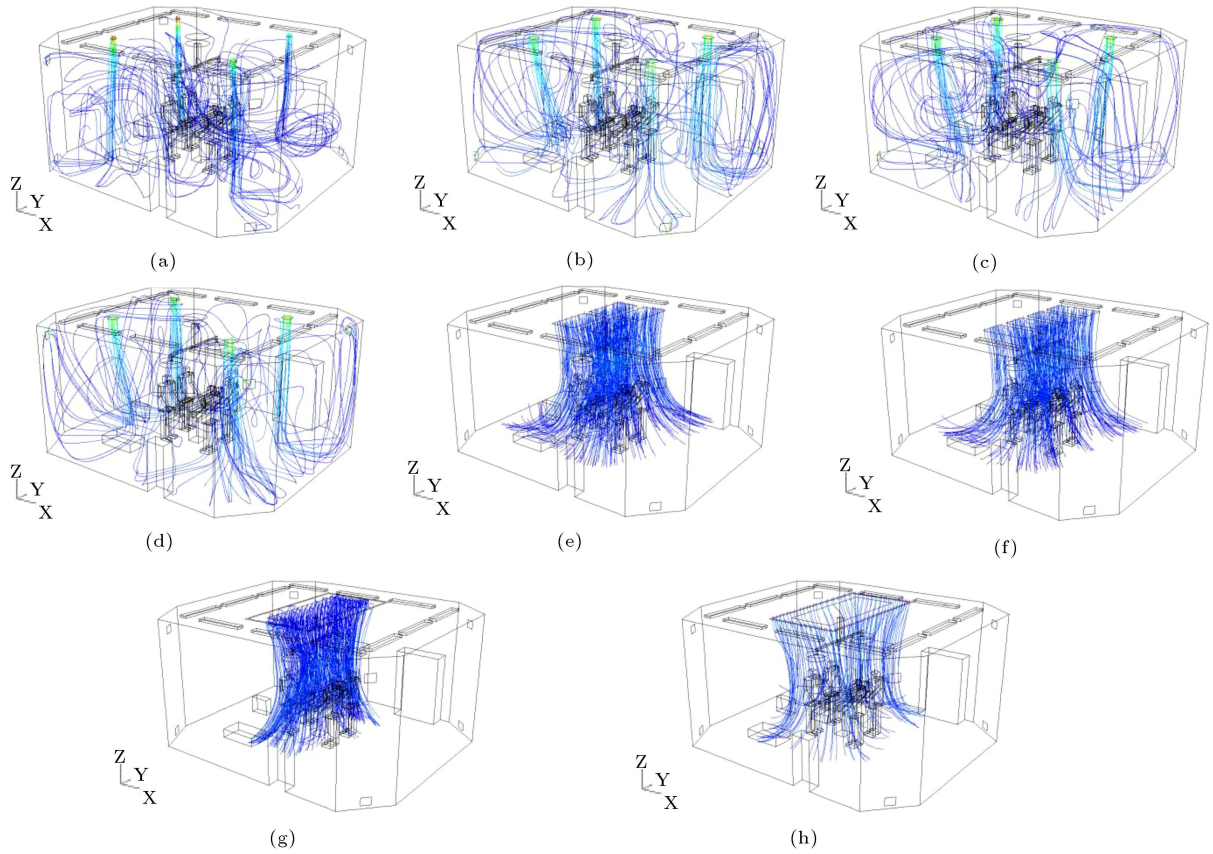


**Figure 8.** Flow pattern: (a) Model 1, (b) model 2, (c) model 3, (d) model 4, (e) model 5, (f) model 6, (g) model 7 (main diffuser), and (h) model 7 (liner diffuser).

entry of unwanted flows from outside the SZ, which is usually associated with pollution. Therefore, it continuously provides clean air to the patient and the surgical team.

### *3.2. Velocity vectors*

The velocity vectors for the central plane passing through the center of the surgical site and the longitudinal direction of the patient's body are shown in Figure 9. In model 1, due to the different velocities of the inlet diffusers, velocity vectors without specific regularity are observed in different directions, indicating turbulent flow for the interior. In this model, the direction of flow is from the surrounding area to the SZ and then, upward. This movement of flow increases the risk of contaminants penetrating the area. In this model, the rotation of the flow in different directions causes the inlet air to mix with the polluted air, thus maximizing the OR space's contamination.

In models 2 to 4 (Figure 9), the flow direction is downward in the SZ; however, it is not directly supplied to the SZ. The flow has a high turbulence and turbulence increases the probability of particle concentration in the space in these models, while its value is not as much as that in model 1. Models 5 to 7 (see Figure 9) directly supply the air to the SZ and provide a laminar and unidirectional flow for this area. The LAF in models 5 to 7 has caused a regular pattern of airflow. Since rotation in this area is minimized, the concentration of pollutants in this area would be lower than that in the surrounding area. The effect of air curtain (model 7) is shown in Figure 9(g). The model's air curtain controls the main diffuser flow and guides it towards the SZ. Another effect of the created air curtain is to prevent the penetration of external flows into the SZ.

Figure 10 shows the distribution of the velocity and concentration of contaminants on the plane $X = 3.053$ m at 2.24 m above the floor just below the surgical lights. As shown in Figure 10(a), a low flow velocity under the surgical lights was observed, and a flow stagnation could be considered in this area. As illustrated in Figure 10(b), the input diffusers are far from the surgical lights in TAF models; therefore, the stagnant flows cause the accumulation of contaminants under the surgical lights. However, in LAF models, since the surgical lights are located directly below the inlet diffusers, the accumulation of contaminants under them is less than TAF models. Therefore, in all the examined models, the effects of surgical lights on the flow pattern cannot be ignored.

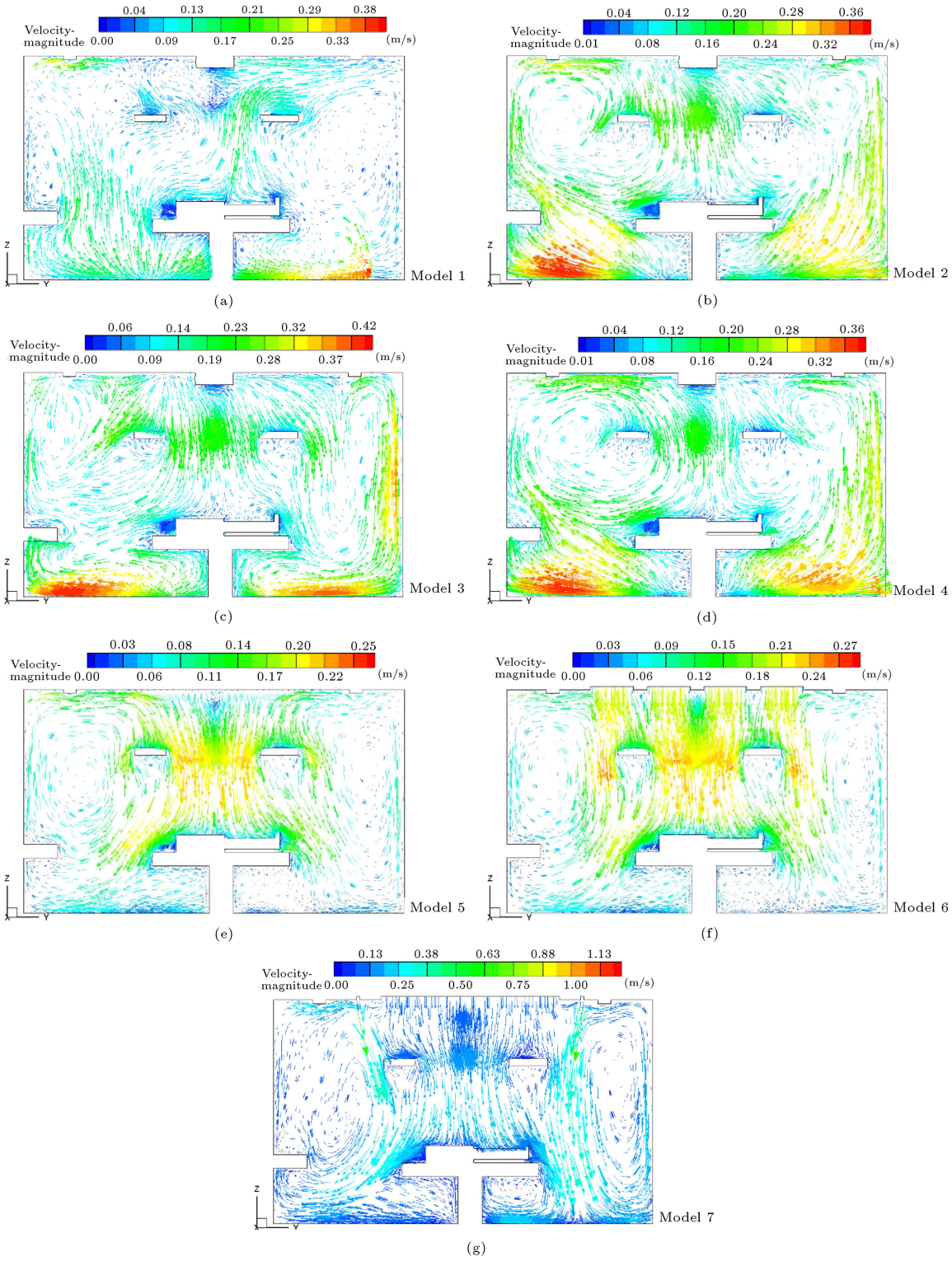


**Figure 9.** Velocity vectors in plane $X = 3.17$ m: (a) Model 1, (b) model 2, (c) model 3, (d) model 4, (e) model 5, (f) model 6, and (g) model 7.

### *3.3. Pressure distribution*

Figure 11 shows the pressure distribution for different $X$ planes covering the SZ and inlet diffusers. Indoor air pressure is an essential factor to prevent the penetration of external contaminants into the OR; therefore, the ASHRAE standards [35] recommend a positive pressure for the indoor air. A negative pressure was observed around the inlet diffusers in model 1 and this is the disadvantage of TAF systems. The resulting negative pressure makes the contaminated air to be

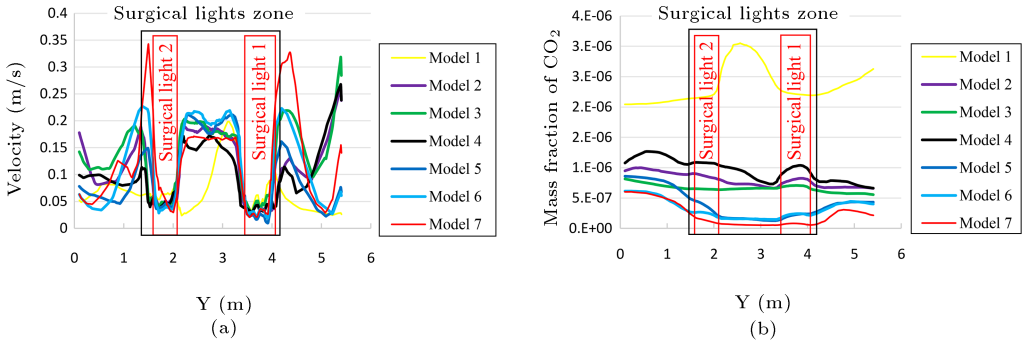


**Figure 10.** Air velocity and $CO_2$ distribution: (a) Velocity distribution for plane $X = 3.053$ m at 2.24 m above floor. (b) $CO_2$ distribution for plane $X = 3.053$ m at 2.24 m above floor.

pushed into the inlet diffusers and blend in with the inlet fresh outdoor air, resulting in the contamination of the incoming air. This air movement prevents the fresh airflow from entering into the SZ and exposes the patient and the surgical personals to contamination. The negative pressure around the diffusers is modified in subsequent design models so that there is no negative pressure around the diffusers for models 2 to 7.

For the center plane in model 1, there is a minimal pressure difference, which increases the risk of contaminant infiltration. In models 2 to 4 (Figure 11), the pressure is high, causing the patient and surgical team to be dissatisfied. The pressure distribution along the patient's body length, i.e., the central plane for the LAF system (see Figure 11), shows a positive pressure difference relative to the surrounding environment. This positive pressure in the SZ causes contaminants originated from people to move continuously to the surrounding environment with a lower pressure level and minimizes the contaminant infiltration into SZ. Models 5 and 6 are the most suitable models to create positive pressure for the OR interior.

### *3.4. The $CO_2$ concentration*

Figure 12 shows the distribution of $CO_2$ concentration at two heights of 1.14 m and 1.7 m above the floor, as the usual heights for the patient and the surgical team. Figure 12(a) shows the distribution of $CO_2$ concentration for plane $X = 3.09$ m at 1.14 m above the floor. The maximum concentration is observed directly above the patient's mouth due to the outflow of breath from the patient's mouth. It was found that the highest concentration occurred in model 1.

Figure 12(b) and (c) shows the distribution of $CO_2$ concentration for the two planes of $X = 3.09$ m and $Y = 2.866$ m at the respiratory height of the surgical team. It was observed that model 1 had the highest level of pollution. In this model, the SZ has a higher $CO_2$ concentration than the surrounding area, and the accumulation of contaminants in the SZ is significant; therefore, it exposes the patient and the surgical personals to the infection. It was found that the LAF models (models 5 to 7) could provide a more appropriate $CO_2$ concentration distribution than the TAF models (models 1 to 4). In all LAF models, the $CO_2$ concentration distribution in the SZ was lower than the surrounding area due to the direct supply airflow to this area.

The most appropriate model among all the examined models is the LAF with the air curtain model (model 7). The air curtain around the SZ causes a barrier to the SZ and prevents the penetration of pollutants and external particles. This creates a sterile area for the surgical personals, the patient, and the SZ and they are not exposed to contaminated air. According to the $CO_2$ concentration analysis, model 7 configuration had a minimum $CO_2$ concentration in the indoor space. It was concluded that model 7 could decrease the mean $CO_2$ concentration value by about 64.66% on plane $X = 3.09$ m at 1.14 m above the floor, 88.96% on plane $X = 3.09$ m at 1.7 m above the floor, and 83.82% on plane $Y = 2.866$ m at 1.7 m above the floor.

The $CO_2$ concentration distribution for plane $Z = 1.14$ m (patient's respiratory height) and plane $Z = 1.7$ m (surgical team's respiratory height) is shown in Figures 13 and 14. The patient's and surgical team's respiratory areas have the highest concentration due to the breath outflow. Comparison of LAF and TAF models shows that LAF models have a lower concentration of contaminant than TAF models. The highest $CO_2$ concentration occurred in model 1, while model 7 had the lowest concentration, indicating the success of the LAF with the air curtain model compared to the other studied models.

## 4. Conclusions

In the present research, the effect of TAF and LAF systems on the air and $CO_2$ distribution in an Operating Room (OR) was studied. The effect of inlet and outlet patterns was examined in the case of seven different models. Computational Fluid Dynamic (CFD) method was employed for this purpose. Flow pattern analysis

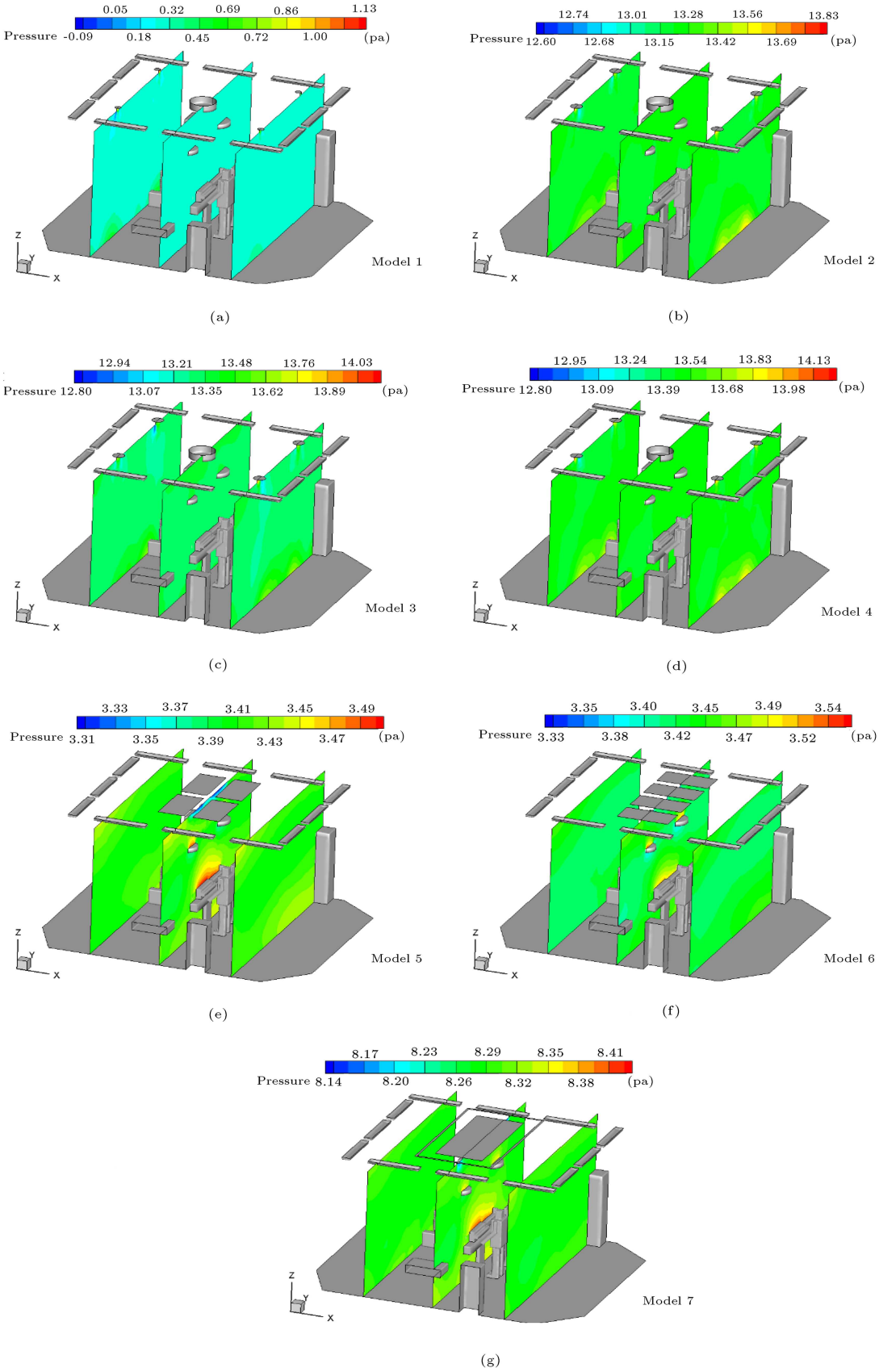


**Figure 11.** Pressure distribution in planes $X = 1.54$ m, $X = 3.17$ m, $X = 4.873$ m: (a) Model 1, (b) model 2, (c) model 3, (d) model 4, (e) model 5, (f) model 6, and (g) model 7.

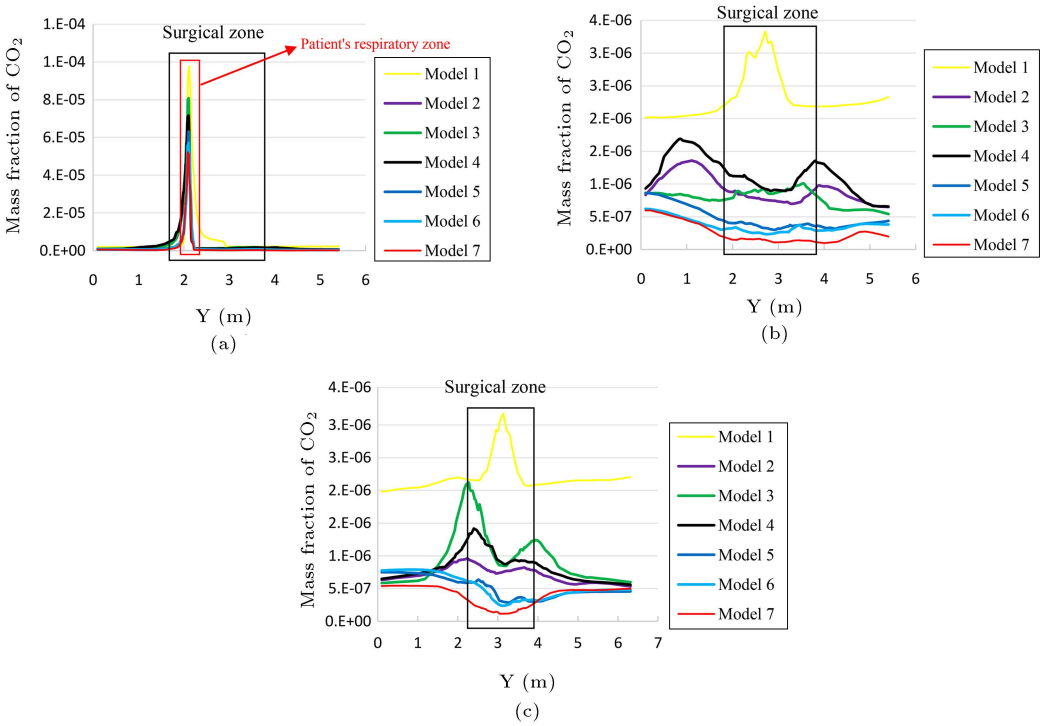


**Figure 12.** $CO_2$ concentration: (a) Plane $X = 3.09$ m at 1.14 m above the floor, (b) plane $X = 3.09$ m at 1.7 m above the floor, and (c) plane $Y = 2.866$ m at 1.7 m above the floor.

for the all examined models showed that in models 1 to 4 (TAF models), a significant fraction of the flow was discharged directly through the outlet vents, and a small fraction of the flow moved to the Surgical Zone (SZ). In these models, due to the lack of flow pattern control, the inlet air was mixed with the polluted air, thus increasing the room's pollution. However, it was shown that the path lines of models 5 to 7 (LAF models) could provide a controllable flow pattern for the SZ and expose the area to the fresh air. The flow pattern of model 7 is more controllable than the other models due to air curtains around the main diffuser. The air curtain around the main diffuser and the SZ acts as a physical barrier and prevents the dissemination of the main diffuser flow and contaminated air entering the SZ.

In all the examined models, the effects of surgical lights were also considered. Airflow collides with the surgical lights, causing turbulence and rotation beneath them. Rotating the flow under the surgical lights disrupts the unidirectional flow of the SZ and causes a stagnant area, which increases the contamination level.

In general, the following results can be expressed for the present study:

(i) The LAF models (models 5 to 7) provided the most appropriate flow pattern for the room, especially the SZ, and it could be stated that the LAF with the air curtain model created the most appropriate flow pattern;

(ii) Model 1 was the most inappropriate one in terms of pressure distribution due to the negative pressure created around the inlet diffusers, while LAF Models 5 and 6 were the best models to generate positive internal pressure;

(iii) The velocity distribution and direction of its vectors in turbulent models were inadequate so that a stagnant space was created in the SZ and the velocity vectors were in different directions. However, the LAF models created a suitable velocity distribution that is unidirectional for the SZ;

(iv) Model 1 had the highest $CO_2$ concentration in the room space, particularly in the SZ, and this showed the inadequacy of the existing model. The LAF models provided lower contaminant concentration levels for the OR, and the LAF with the air curtain model was the most appropriate;

(v) The effects of surgical lights on the flow distribution were also considered. The thermal plume around these lights and the rotation of flow beneath them were the effects of the presence of surgical lights.

## Acknowledgments

The authors would like to acknowledge Chabahar Maritime University (CMU), Iran and Chabahar Ira-

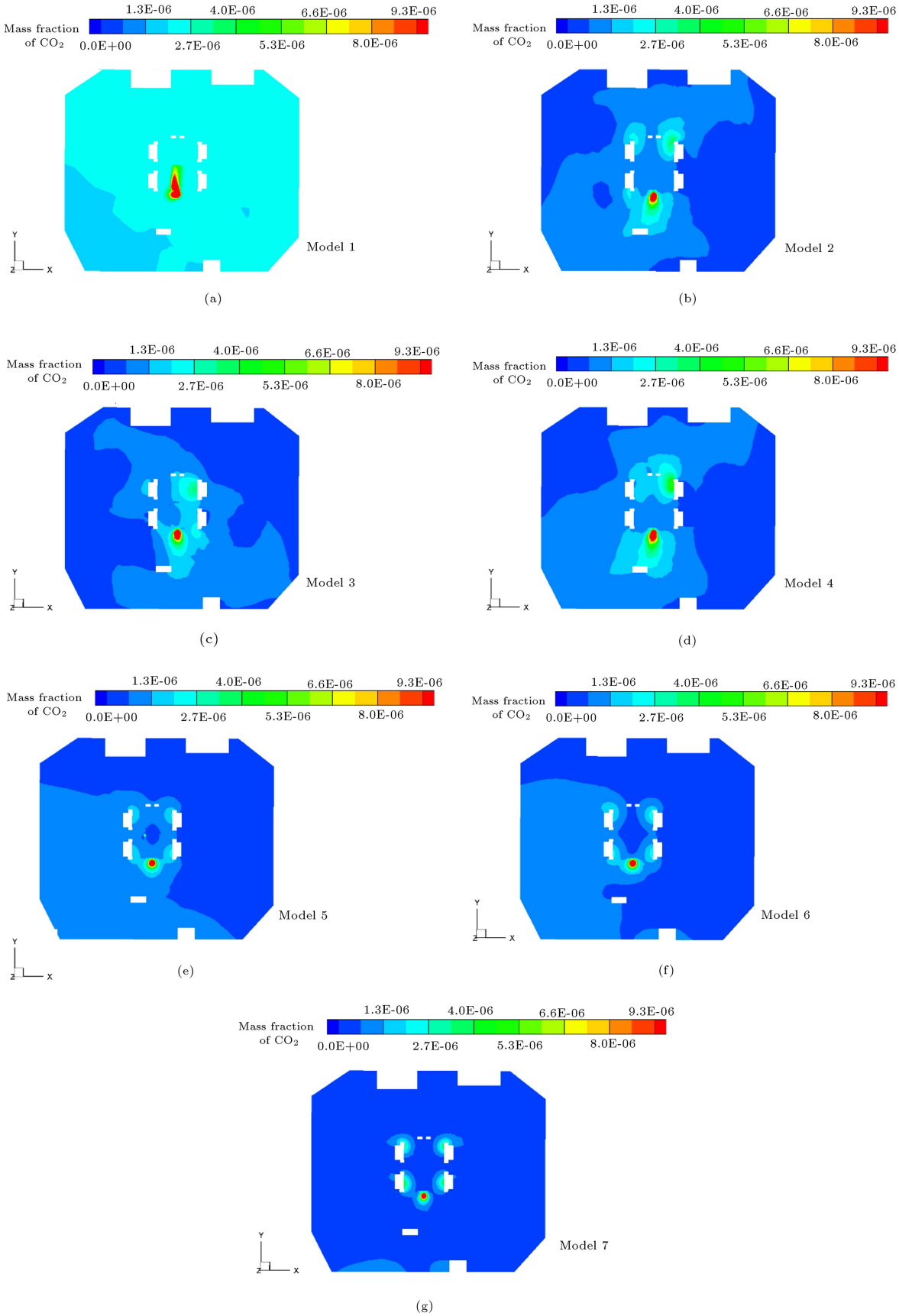


**Figure 13.** $CO_2$ distribution in plane $Z = 1.14$ m (patient's respiratory height): (a) Model 1, (b) model 2, (c) model 3, (d) model 4, (e) model 5, (f) model 6, and (g) model 7.

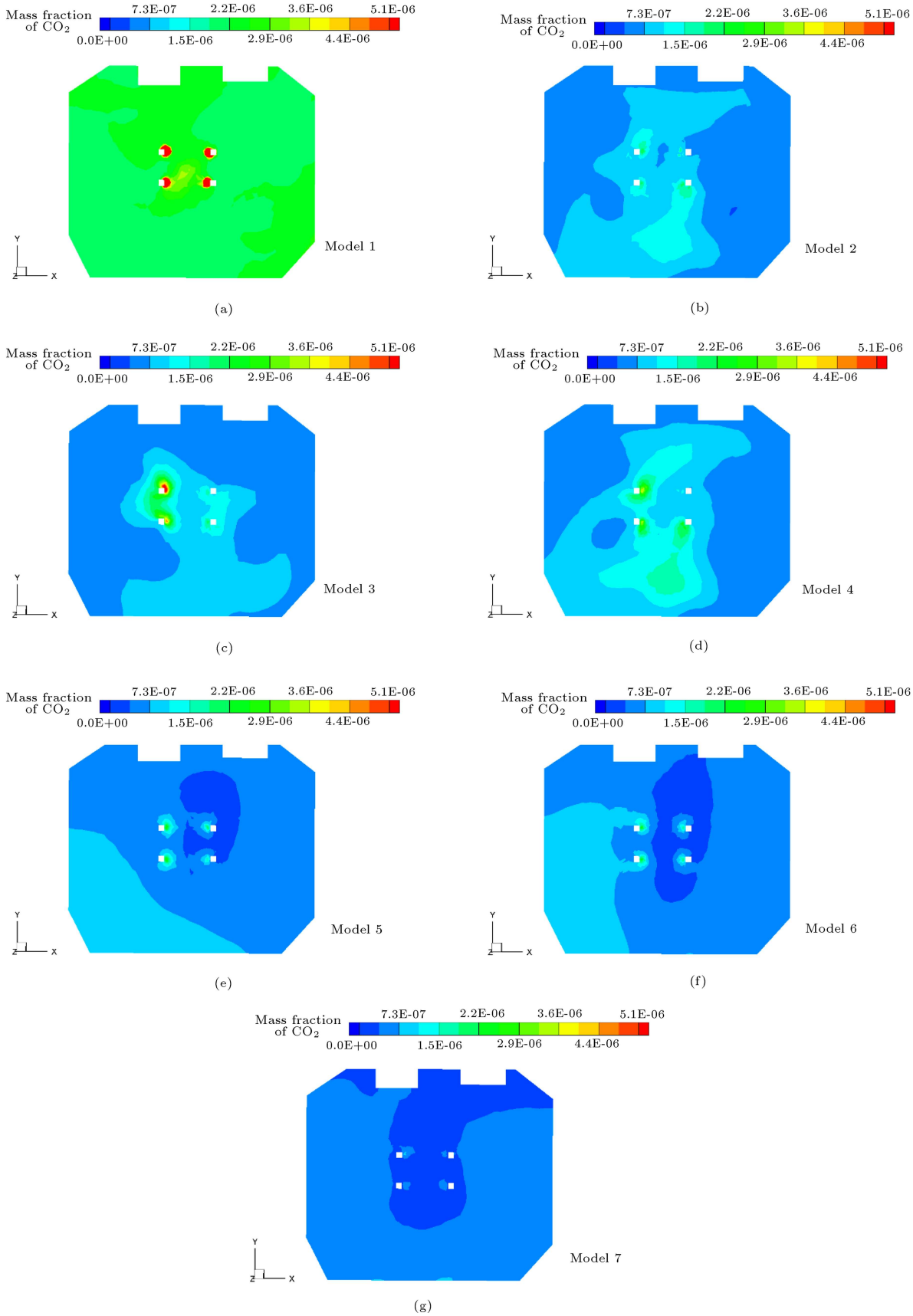


**Figure 14.** $CO_2$ distribution in plane $Z = 1.7$ m (surgical team's respiratory height): (a) Model 1, (b) model 2, (c) model 3, (d) model 4, (e) model 5, (f) model 6, and (g) model 7.

nian Surgery Clinic for their cooperation during the research.

## Nomenclature

| | |
|---|---|
| $C$ | Constant |
| $D$ | Coefficient of molecular diffusivity |
| $D_t$ | Coefficient of turbulent molecular diffusivity |
| $E$ | Total energy (J) |
| $G_b$ | Turbulence kinetic energy generated by buoyancy |
| $G_k$ | Turbulence kinetic energy generated by the mean velocity gradients |
| $g$ | Gravity acceleration ($m/s^2$) |
| $h$ | Enthalpy (J) |
| $k$ | Turbulence kinetic energy ($m^2/s^2$) |
| $K_{eff}$ | Effective conductivity (W/m.K) |
| $P$ | Static pressure (Pa) |
| $S$ | Source terms |
| $S_i$ | The contaminant generation rate |
| $T$ | Temperature (K) |
| $V$ | Velocity (m/s) |
| $\vec{v}$ | Velocity vector (m/s) |
| $Y_M$ | Contribution of the fluctuating dilatation |

### *Greek symbols*

| | |
|---|---|
| $\nu$ | Kinematic viscosity ($m^2/s$) |
| $\mu$ | Dynamic viscosity (kg/ms) |
| $\mu_{eff}$ | Turbulent viscosity coefficient (kg/ms) |
| $\mu_t$ | Turbulence viscosity (kg/ms) |
| $\rho$ | Fluid density ($kg/m^3$) |
| $\rho_o$ | Specified density of air ($kg/m^3$) |
| $\rho_\beta$ | Boussinesq density ($kg/m^3$) |
| $\bar{\bar{\tau}}$ | Stress tensor (Pa) |
| $\bar{\bar{\tau}}_{eff}$ | Deviatoric stress tensor (Pa) |
| $\beta$ | Thermal expansion coefficient ($k^{-1}$) |
| $\sigma_k$ | Turbulent Prandtl number for $k$ |
| $\sigma_\varepsilon$ | Turbulent Prandtl number for $\varepsilon$ |
| $\varepsilon$ | Rate of dissipation ($m^2/s^3$) |
| $\bar{Y}_i$ | Species concentration |

### *Abbreviations*

| | |
|---|---|
| ACH | Air Change rate per Hour |
| ASHRAE | American Society of Heating, Refrigerating and Air-conditioning Engineers |
| BCPs | Bacteria-Carrying Particles |
| CFD | Computational Fluid Dynamic |
| CFUs | Colony-Forming Units |
| HVAC | Heating, Ventilation and Air Conditioning |
| IJV | Impinging Jet Ventilation |
| ISC | Iranian Surgery Clinic |
| LAF | Laminar Airflow |
| OR | Operating Room |
| PIV | Particle Image Velocimetry |
| RH | Relative Humidity |
| SARS-CoV-2 | Severe Acute Respiratory Syndrome Corona Virus 2 |
| SLD | Single Large Diffuser |
| SSIs | Surgical Site Infections |
| SZ | Surgical Zone |
| TAF | Turbulent Airflow |
| UCV | Ultra Clean Ventilation |
| UFPs | Ultra Fine Particles |

## References

1. Berríos-Torres, S.I., Umscheid, C.A., Bratzler, D.W., et al. "Centers for disease control and prevention guideline for the prevention of surgical site infection, 2017", *JAMA Surg.*, **152**(8), pp. 784–791 (2017).
2. Coello, R., Charlett, A., Wilson, J., et al. "Adverse impact of surgical site infections in English hospitals", *J. Hosp. Infect.*, **60**(2), pp. 93–103 (2005).
3. Sadeghian, P., Wang, C., Duwig, C., et al. "Impact of surgical lamp design on the risk of surgical site infections in operating rooms with mixing and unidirectional airflow ventilation: A numerical study", *Journal of Building Engineering*, **31**, p. 101423 (2020).
4. Loomans, M., De Visser, I., Loogman, J., et al. "Alternative ventilation system for operating theaters: Parameter study and full-scale assessment of the performance of a local ventilation system", *Build. Environ.*, **102**, pp. 26–38 (2016).
5. Liu, Z., Liu, H., Rong, R., et al. "Effect of a circulating nurse walking on airflow and bacteria-carrying particles in the operating room: An experimental and numerical study", *Build. Environ.*, **186**, p. 107315 (2020).
6. De Lissovoy, G., Fraeman, K., Hutchins, V., et al. "Surgical site infection: incidence and impact on hospital utilization and treatment costs", *Am. J. Infect. Control*, **37**(5), pp. 387–397 (2009).
7. Chow, T.-T. and Wang, J. "Dynamic simulation on impact of surgeon bending movement on bacteria-carrying particles distribution in operating theatre", *Build. Environ.*, **57**, pp. 68–80 (2012).

8. Andersson, A.E., Bergh, I., Karlsson, J., et al. "Traffic flow in the operating room: an explorative and descriptive study on air quality during orthopedic trauma implant surgery", *Am. J. Infect. Control*, **40**(8), pp. 750–755 (2012).

9. Darouiche, R.O., Green, D.M., Harrington, M.A., et al. "Association of airborne microorganisms in the operating room with implant infections: a randomized controlled trial", *Infect. Control Hosp. Epidemiol.*, **38**(1), pp. 3–10 (2017).

10. Stocks, G.W., Self, S.D., Thompson, B., et al. "Predicting bacterial populations based on airborne particulates: a study performed in nonlaminar flow operating rooms during joint arthroplasty surgery", *Am. J. Infect. Control*, **38**(3), pp. 199–204 (2010).

11. Stocks, G.W., O'connor, D.P., Self, S.D., et al. "Directed air flow to reduce airborne particulate and bacterial contamination in the surgical field during total hip arthroplasty", *J. Arthroplasty*, **26**(5), pp. 771–776 (2011).

12. Cook, M., *The Design Quality Manual: Improving Building Performance*, John Wiley & Sons (2008).

13. Mcneill, J., Hertzberg, J., and Zhai, Z.J. "Experimental investigation of operating room air distribution in a full-scale laboratory chamber using particle image velocimetry and flow visualization", *J. Flow Control, Meas. Visualization*, **1**(1), pp. 24–32 (2013).

14. Cao, G., Nilssen, A.M., Cheng, Z., et al. "Laminar airflow and mixing ventilation: Which is better for operating room airflow distribution near an orthopedic surgical patient?", *Am. J. Infect. Control*, **47**(7), pp. 737–743 (2019).

15. Stacey, A. and Humphreys, H. "A UK historical perspective on operating theatre ventilation", *J. Hosp. Infect.*, **52**(2), pp. 77–80 (2002).

16. Whyte, W., Hodgson, R., and Tinkler, J. "The importance of airborne bacterial contamination of wounds", *J. Hosp. Infect.*, **3**(2), pp. 123–135 (1982).

17. Lidwell, O., Lowbury, E., Whyte, W., et al. "Effect of ultraclean air in operating rooms on deep sepsis in the joint after total hip or knee replacement: a randomised study", *Br. Med. J.*, **285**, pp. 10–14 (1982).

18. Bischoff, P., Kubilay, N.Z., Allegranzi, B., et al. "Effect of laminar airflow ventilation on surgical site infections: a systematic review and meta-analysis", *Lancet Infect. Dis.*, **17**(5), pp. 553–561 (2017).

19. Andersson, A.E., Petzold, M., Bergh, I., et al. "Comparison between mixed and laminar airflow systems in operating rooms and the influence of human factors: experiences from a Swedish orthopedic center", *Am. J. Infect. Control*, **42**(6), pp. 665–669 (2014).

20. Wang, C., Holmberg, S., and Sadrizadeh, S. "Numerical study of temperature-controlled airflow in comparison with turbulent mixing and laminar airflow for operating room ventilation", *Build. Environ.*, **144**, pp. 45–56 (2018).

21. Alonso, J.S.J., Sanz-Tejedor, M., Arroyo, Y., et al. "Analysis and assessment of factors affecting air inflow from areas adjacent to operating rooms due to door opening and closing", *Journal of Building Engineering*, **49**, p. 104109 (2022).

22. Gholami Motlagh, V. and Ahmadzadehtalatapeh, M. "Optimization of air distribution patterns by arrangements of air inlets and outlets: Case study of an operating room", *J. Appl. Comput. Mech.*, **8**(3), pp. 809–830 (2022).

23. Liu, Z., Yin, D., Hu, L., et al. "Bacteria-carrying particles diffusion in the operating room due to the interaction between human thermal plume and ventilation systems: An experimental-numerical simulation study", *Energy Build.*, **270**, p. 112277 (2022).

24. Fan, M., Cao, G., Pedersen, C., et al. "Suitability evaluation on laminar airflow and mixing airflow distribution strategies in operating rooms: A case study at St. Olavs Hospital", *Build. Environ.*, **194**, p. 107677 (2021).

25. Zhai, Z.J. and Osborne, A.L. "Simulation-based feasibility study of improved air conditioning systems for hospital operating room", *Frontiers of Architectural Research*, **2**(4), pp. 468–475 (2013).

26. ASHRAE, ANSI Standard 170-2008 Ventilation of Health Care Facilities, American Society of Heating, Refrigerating and Air-Conditioning Engineers, Inc, Atlanta (2008).

27. Ning, M., Mengjie, S., Mingyin, C., et al. "Computational fluid dynamics (CFD) modelling of air flow field, mean age of air and $CO_2$ distributions inside a bedroom with different heights of conditioned air supply outlet", *Appl. Energy*, **164**, pp. 906–915 (2016).

28. Ufat, H., Kaynakli, O., Yamankaradeniz, N., et al. "Three-dimensional air distribution analysis of different outflow typed operating rooms at different inlet velocities and room temperatures", *Adv. Mech. Eng.*, **9**(7), pp. 1–12 (2017).

29. Deng, H.-Y., Feng, Z., and Cao, S.-J. "Influence of air change rates on indoor $CO_2$ stratification in terms of Richardson number and vorticity", *Build. Environ.*, **129**, pp. 74–84 (2018).

30. Yau, Y. and Ding, L. "A case study on the air distribution in an operating room at Sarawak General Hospital Heart Centre (SGHHC) in Malaysia", *Indoor Built Environ.*, **23**(8), pp. 1129–1141 (2014).

31. Ding, L. and Yau, Y. "A study on the arrangement of air inlets in a Class 7 clean room", *Building Serv. Eng. Res. Technol.*, **36**(3), pp. 357–367 (2015).

32. Zheng, C., You, S., Zhang, H., et al. "Comparison of air-conditioning systems with bottom-supply and side-supply modes in a typical office room", *Appl. Energy*, **227**, pp. 304–311 (2018).

33. Liu, J., Wang, H., and Wen, W. "Numerical simulation on a horizontal airflow for airborne particles control in hospital operating room", *Build. Environ.*, **44**(11), pp. 2284–2289 (2009).

34. Tung, Y.-C., Shih, Y.-C., and Hu, S.-C. "Numerical study on the dispersion of airborne contaminants from an isolation room in the case of door opening", *Appl. Therm. Eng.*, **29**(8–9), pp. 1544–1551 (2009).

35. ASHRAE, ANSI Standard 170-2013 Ventilation of Health Care Facilities, American Society of Heating, Refrigerating and Air-Conditioning Engineers, Inc, Atlanta (2013).

## Biographies

**Vahid Gholami Motlagh** received MSc degree in Mechanical Engineering from Chabahar Maritime University, Chabahar, Iran in 2018. He is a Research Assistant at Chabahar Maritime University. His major interest areas are air-conditioning systems; HVAC & R Engineering; computational fluid dynamics; infection control in indoor spaces.

**Mohammad Ahmadzadehtalatapeh** received the PhD degree in Mechanical Engineering from Malya University, Kuala Lumpur, Malaysia in 2011. Presently, he is an Associate Professor at the Chabahar Maritime University, Chabahar, Iran. His major interest areas are air-conditioning systems, HVAC & R Engineering; thermal systems simulation using TRNSYS; energy savings in buildings; heat exchangers, heat pipe heat exchangers.

**Omid Mohammadi** received MSc degree in Mechanical Engineering from Sharif University, Tehran, Iran in 2019. He is a Research Assistant at Sharif University of technology. His major interest areas are renewable energies; thermal energy storage; ventilation.